Numerical Calculation of Unsteady Transonic Potential Flow over Helicopter Rotor Blades

Francis X. Caradonna*
NASA Ames Research Center, Moffett Field, California
and
Morris P. Isom†
Polytechnic Institute of New York Brooklyn, New York

The small disturbance potential equation appropriate to a helicopter in forward flight is derived. This equation then is solved for the flow over a nonlifting transonic rotor blade, using a completely implicit scheme that is an extension of the Murman-Cole mixed difference technique. The flow in the tip region is most unsteady in the decelerating flow region, after the blade passes the $\psi = 90°$ azimuthal station. The unsteadiness appears to be caused by expansion and compression waves that move slowly upstream of the blade as the relative incident flow decelerates. The influence of aspect ratio, advance ratio, and Mach number on this process is discussed.

Introduction

THE onset of transonic flow is one of the primary conditions that sets the performance limits of modern helicopters. Its occurrence is not rare, and not only does it cause performance and vibration problems, but it also is implicated in some of the more objectionable noise situations.

A transonic flow regime near a rotor blade tip is an inherently three-dimensional and nonlinear flowfield, with an embedded supersonic region terminated by a shock wave, and the flow is also unsteady for sufficiently high advance ratios. It is extremely difficult to carry out experimental investigations of transonic rotor aerodynamics. The combination of theoretical and experimental difficulties has left the problem in a poorly understood state.

The first numerical attack on this problem was made in Ref. 1, in which the mixed-difference relaxation method of Murman and Krupp[2] was extended to solve the case of nonlifting hovering rectangular rotor with biconvex sections operating in the lower transonic regime. The tip relief effect was discussed, and it was demonstrated that decreasing aspect ratio with the transonic similarity parameter held fixed had beneficial effects on the supersonic pressure distribution. These result were extended[3] to include some nonrectangular planforms; these variations in geometry were shown to have a large effect on the flow.

The analysis of Ref. 1 is restricted to a rotor with zero-advance ratio, so that the flow is steady in a coordinate system attached to the blade. Here we shall consider the rotor in forward motion. Particular attention is given to a nonlifting, three-dimensional, nonlinear flow regime, with advance ratio sufficiently high to produce unsteady effects.

Formulation and Governing Equations

In the transonic near field, close to the advancing tip region, the flow is not influenced in a first approximation by other portions of the blade system. Therefore, attention is restricted to the outer few chords of the advancing blade. It will be assumed that the flow is inviscid and isentropic. A velocity potential therefore exists for the flow described in an inertial coordinate system. This system is taken to be one at rest, relative to the undisturbed air. The equation for the velocity potential ϕ in the rest frame is

$$\phi_{t't'} + \frac{\partial}{\partial t'}(\nabla'\phi)^2 + \nabla'\phi \cdot \nabla'[\tfrac{1}{2}(\nabla'\phi)^2] = a^2\nabla'^2\phi \qquad (1)$$

where a is the local adiabatic sound speed. Bernoulli's equation relating a and ϕ is

$$\phi_{t'} + \tfrac{1}{2}(\nabla'\phi)^2 + [a^2/(\gamma-1)] = [a_\infty^2/(\gamma-1)] \qquad (2)$$

a_∞ is the sound speed in undisturbed air, and γ is the ratio of specific heats. A prime on the time variable t' and the gradient operator in Eqs. (1) and (2) refers to the fixed reference frame (see Fig. 1); it distinguishes these quantities from their counterparts in a translating and rotating frame, to be introduced later. Relative to a fixed Cartesian (x', y', z') coordinate system, the blade geometry and location are described by $F(x', y', z', t') = 0$. The condition of flow tangency at the blade surface is

$$F_{t'} + \nabla'\phi \cdot \nabla' F = 0 \qquad (3)$$

We require that $\phi_{t'}$ and $\nabla'\phi$ go to zero at infinity.

In all cases of interest here (including nonlinear problems), the third term on the left-hand side of Eq. (1), the cubic term, is negligible. That term will be neglected in all further discussion.

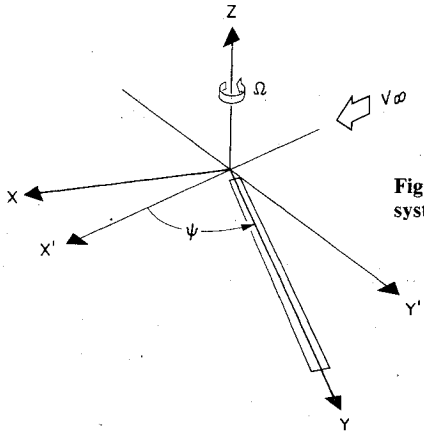

Fig. 1 Rotor coordinate system.

Presented as Paper 75-168 at the AIAA 13th Aerospace Sciences Meeting, Pasadena, Calif., Jan. 20-22, 1975; submitted March 3, 1975; revision received Aug. 25, 1975.

Index categories: Nonsteady Aerodynamics; Subsonic and Transonic Flow; Rotary Wing Aerodynamics.

*Research Scientist, U.S. Army Air Mobility R/D Lab. Member AIAA.

†Associate Professor, Aerospace Engineering and Applied Mechanics.

It is convenient to reformulate the problem in a coordinate system attached to the blade, with the origin at the center of rotation. The velocity of advance V_0' is in the direction of the negative x' axis of the fixed reference frame. Coordinate z for both fixed and moving frames is normal to the plane of rotation, and the angular velocity of rotation Ω points in the positive z direction. In the rotating frame, the blade-attached x axis is in the chordwise direction, and the y axis is along the blade span. Let $r'=(x', y', z')$ and $r=(x, y, z)$ be position vectors in the fixed and moving frames. The two reference frames coincide at time $t=0$ and are related by

$$r'=V_0't+R(t)r$$
$$t'=t$$

where $R(t)$ is the rotation matrix

$$R(t)=\begin{bmatrix} \cos\Omega t & -\sin\Omega t & 0 \\ \sin\Omega t & \cos\Omega t & 0 \\ 0 & 0 & 1 \end{bmatrix}$$

With this transformation, time derivatives in the fixed and moving frames are related by

$$(\partial\phi/\partial t')=(\partial\phi/\partial t)-(\Omega xr+V_0)\cdot\nabla\phi \tag{4}$$

The velocity V in Eq. (4) must be expressed as it appears to an observer in the moving frame. In the fixed frame, $V_0'=-i'V_0$, with i a unit vector along the fixed x' axis. In the moving frame,

$$V_0=-iV\cos\Omega t+jV\sin\Omega t \tag{5}$$

where i and j are unit vectors in the positive x and y directions of the blade-fixed system. The observer in the moving frame thus sees a freestream velocity

$$V=-V_0-\Omega\times r \tag{6}$$

and time derivatives of Eq. (4) are related by

$$\partial\phi/\partial t'=(\partial\phi/\partial t)+V\cdot\nabla\phi \tag{7}$$

Use of Eq. (7) in Eqs. (1) and (2) gives the differential equation for ϕ in the blade-fixed coordinate system:

$$\phi_{tt}+V\cdot\nabla\nabla\phi\cdot V+2V\cdot\nabla\phi_t-\Omega xV\cdot\nabla\phi$$
$$-V\cdot\nabla\phi+2\nabla\phi\cdot\nabla\phi_t+2V\cdot\nabla\nabla\phi\cdot\nabla\phi$$
$$=\{a_\infty^2-(\gamma-1)[\phi_t+V\cdot\nabla\phi+\tfrac{1}{2}(\nabla\phi)^2]\}\nabla^2\phi \tag{8}$$

A preliminary simplification of Eq. (8) will not be made, and it can be verified later that terms dropped here are negligible. All first-order derivatives on the left-hand side of Eq. (8) may be neglected. The term $2\nabla\phi\cdot\nabla\phi_t$ may be neglected, compared to the term $2\nabla\cdot\nabla\phi_t$, because V is the zeroth order freestream velocity, and $\nabla\phi$ is a perturbation velocity. On the right-hand side of Eq. (8), the terms ϕ_t and $\tfrac{1}{2}(\nabla\phi)^2$ are negligible. With these observations, the basic Eq. (8) becomes

$$\phi_{tt}+V\cdot\nabla\nabla\phi\cdot V+2V\cdot\nabla\phi_t+2V\cdot\nabla\nabla\phi\cdot\nabla\phi$$
$$=[a_\infty^2-(\gamma-1)V\cdot\nabla\phi]\nabla^2\phi \tag{9}$$

The blade surface is stationary in the moving reference frame. Let blade geometry be specified by $z=g(x,y)$. The tangency condition, Eq. (3), is

$$\phi_z(x,y,z,t)=(V+\nabla\phi)\cdot\nabla g$$

evaluated on $z=g(x,y)$. The term $\nabla\phi$ is negligible, and the mean surface approximation gives

$$\phi_z(x,y,o,t)=V\cdot\nabla g \tag{10}$$

with V defined by Eq. (6).

Scaling of Eqs. (9) and (10) requires that they be written out in scalar form. Using the definition of V in Eq. (6) and rearranging some terms, the differential Eq. (9) expands to

$$\phi_{tt}+2(\Omega y+V\cos\Omega t)\phi_{xt}-2(\Omega x+V\sin\Omega t)\phi_{yt}$$
$$=[a_\infty^2-(\Omega y+V\cos\Omega t)^2-(\gamma+1)(\Omega y+V\cos\Omega t)\phi_x$$
$$-(\gamma-1)(\Omega x+V\sin\Omega t)\phi_y]\phi_{xx}+[2(\Omega x+V\sin\Omega t)$$
$$\times(\Omega y+V\cos\Omega t)+2(\Omega x+V\sin\Omega t)\phi_x$$
$$-2(\Omega y+V\cos\Omega t)\phi_y]\phi_{xy}+]a_\infty^2-(\Omega x+V\sin\Omega t)^2$$
$$-(\gamma-1)(\Omega x+V\cos\Omega t)\phi_x+(\gamma+1)$$
$$\times(\Omega x+V\sin\Omega t)\phi_y]\phi_{yy}$$
$$-2(\Omega y+V\sin\Omega t)\phi_z\phi_{xz}+2(\Omega x+2(\Omega x+V\sin\Omega t)\phi_z\phi_{xz}$$
$$+[a_\infty^2-(\gamma-1)(\Omega y+V\cos\Omega t)\phi_x+(\gamma-1)(\Omega x+V\sin\Omega t)]\phi_{zz} \tag{11}$$

The expanded form of the boundary condition, Eq. (10), is

$$\phi_z(x,y,o,t)=(\Omega y+V\cos\Omega t)g_x-(\Omega x+V\sin\Omega t)g_y \tag{12}$$

Equations (11) and (12), with suitable boundary condition at infinity, describe the rotor aerodynamics. These equations can be further simplified by scaling them.

Scaled Equations

The introduction of new symbols for nondimensional scaled variables can be avoided by a convenient notation. The combination Ωt in Eqs. (11) and (12) is simply replaced by t, with the understanding that from now on t stands for Ωt. Similarly, let c be the blade chord and R the blade radius, and use the substitutions $x/c\to x$, $y/R\to y$. The complete set of time and spatial substitutions is then

$$\Omega t\to t \quad x/c\to x \quad y/R\to y$$
$$\tau^{1/3}z/c\to z \quad \phi/\tau^{2/3}\Omega Rc\to\phi \tag{13}$$

where τ is a reference ratio in the tip region. Scaling of the normal coordinate z and the potential ϕ in Eq. (13) is suggested by the usual transonic fixed-wing results, and is the same as that used for the transonic hover problem in Ref. 1. The reference Mach number and advance ratio are

$$M=\Omega R/a_\infty \quad \mu=V/\Omega R \tag{14}$$

The blade has aspect ratio $AR=R/c$, and for a rotor blade we define the small parameter ϵ by

$$\epsilon=AR^{-1} \tag{15}$$

Let blade geometry be further specified in nondimensional form by

$$z=\tau f(x,y) \tag{16}$$

Use of the relations (13-16) in Eqs. (11) and (12), and deletion of some terms by inspection, gives

$$\frac{M^2\epsilon^2}{\tau^{2/3}}\phi_{tt}+2M^2\frac{\epsilon}{\tau^{2/3}}(y+\mu\cos t)\phi_{xt}$$

$$-\frac{2M^2\epsilon^2}{\tau^{2/3}}(\epsilon x+\mu\sin t)\phi_{yt}$$

$$=\left[\frac{1-M^2(y+\mu\cos t)^2}{\tau^{2/3}}-(\gamma+1)M^2\right.$$

$$\left.\times(y+\mu\cos t)\phi_x\right]\phi_{xx}+\frac{2M^2\epsilon}{\tau^{2/3}}(\epsilon x+\mu\sin t)$$

$$\times(y+\mu\cos t)\phi_{xy}+\frac{\epsilon^2}{\tau^{2/3}}\phi_{yy}+\phi_{zz} \tag{17}$$

with the boundary condition

$$\phi_z(x,y,o,t)=(y+\mu\cos t)f_x-\epsilon(\epsilon x+\mu\sin t)f_y \tag{18}$$

Some assumption must be made now about the relative orders of magnitude of $\gamma=\mathcal{R}^{-1}$ and τ. A typical blade has a thickness ratio of about 0.06 to 0.12 near the tip, and the aspect ratio of about 10 to 20. We therefore assume the limits $\tau\to 0$, $\epsilon\to 0$, $\tau/\epsilon=0(1)$. The advance ratio is assumed to be about 0.2 to 0.4, and is held fixed when any limits are taken.

When the flow is transonic only on the advancing side of the rotor disk, there is some finite azimuthal angle, measured at $t=0$, within which the flow is transonic and outside of which the flow should become subsonic. It is necessary therefore to scale time in a suitable way. Also, when the flow is transonic, there is a characteristic region near the tip, measured in chords, within which the flow is transonic and inboard of which the flow becomes subsonic and follows strip theory. Following Ref. 1, a transonic span variable is

$$S=\tau^{1/3}[(1-y)/\epsilon]\quad y=1-(\epsilon/\tau^{1/3})S \tag{19}$$

A scaled time variable T for the transonic region is

$$t=\tau^{1/3}T \tag{20}$$

Transonic conditions exist for scaled variables $S=0(1)$, $T=0(1)$. We now substitute Eqs. (19) and (20) into Eqs. (17) and (18), and assume

$$\tau\to 0\quad \epsilon\to 0\quad \epsilon/\tau=0(1)\quad (1-M_T^2)/\tau^{2/3}=0(1)$$

where $M_T=M(1+\mu)$ is the freestream Mach number at the advancing blade tip. The differential equation and boundary condition become

$$2M^2(1+\mu)\frac{\epsilon}{\tau}=\left[\frac{1-M_T^2}{\tau^{2/3}}+2M^2(1+\mu)\frac{\epsilon}{\tau}S\right.$$

$$\left.M^2(1+\mu)\mu T^2-(\gamma+1)M^2(1+\mu)\phi_x\right]\phi_{xx}$$

$$-2M^2\mu(1+\mu)T\phi_{xS}+\phi_{SS}+\phi_{zz} \tag{21}$$

and

$$\phi_z(x,S,o,T)=(1+\mu)f_x \tag{22}$$

The original choice of the relative orders of magnitude of ϵ and τ was based on the observation that $\epsilon=0(\tau)$ for a typical rotor blade. It now emerges from Eq. (21) that, analytically, a necessary condition for the flow to be transonic and nonlinear is that this relation between ϵ and τ should hold.

The transonic problem defined by Eqs. (21) and (22) differs from a subsonic problem in two essential respects: the transonic problem is nonlinear (in the usual way), and it is essentially an unsteady problem with the coefficient of $\phi_{xT}=0(1)$. Thus, the simplifying feature of quasisteady flow does not appear. This latter result naturally complicates numerical calculations because solutions must be obtained in a four-dimensional (x,y,z,t) space. The term in ϕ_{TT}, however, does not appear. The hypersurface $T=$const (or $t=$const) therefore is characteristic.

There are two groups of terms in Eq. (21) that indicate the amount of unsteadiness. The left-hand side does so directly. The coefficient of the ϕ_{xx} term does so indirectly in that, if any of the linear terms therein become large with respect to the nonlinear term ϕ_x, the problem can be rescaled in the subsonic manner, and it becomes quasisteady. In this case time would enter only as a parameter, the flow exhibiting no history effects. Also, the effect of decreasing Mach number is clearly to make the problem steadier and more linear, as it both decreases the coefficient of the unsteady term and increases the transonic similarity parameter. The effect of increasing ϵ/τ is not so clear, however. As a coefficient of ϕ_{xT}, it has the effect of a reduced frequency: if thickness ratio τ is held fixed while aspect ratio is decreased so that ϵ is increased, ϵ/τ also multiplies the transonic span variable S in the coefficient of ϕ_{xx}. As ϵ/τ becomes larger, the relative importance of the nonlinear term is reduced. This effect produces a trend toward subsonic, quasisteady flow.

The effects of similarity parameter, thickness ratio, and aspect ratio are displayed completely in the differential equation [Eq. (21)], scaled for the tip region. These parameters do not appear in the tip boundary condition Eq. (22), nor do they appear to lowest order in the inner boundary condition, Eq. (18). The same cannot be said of advance ratio μ. This parameter appears in Eq. (18), in the tip boundary condition Eq. (22), and also to lowest order in the inner boundary condition Eq. (18). The potential ϕ could be rescaled to eliminate μ from both the inner boundary condition, Eq. (18) (to lowest order in ϵ) and also from Eq. (22). But this rescaling would be accomplished at the expense of increased complexity in Eq. (21). Over all, it would appear that qualitative effects of variation in advance ratio may be read directly from Eq. (21). That equation plausibly suggests that, for fixed maximum tip Mach number M_T, an increase in μ will enhance both the unsteady and the nonlinear terms. However, for the usual values of μ (0.2 to 0.4) the effects are not very large. It is interesting that even when μ goes to zero (the hover case) the unsteady term does not vanish—it must be recognized that the unsteady equations admit a steady solution in this case. Further discussion of scaling the unsteady problem, and the effects of extreme variations in advance ratio and aspect ratio, appear in Ref. 4.

It will be noted that, for the values of advance ratio considered here ($\mu=0.2$ and $\mu=0.4$), the tip flow is transonic, unsteady, and nonlinear over a sector of the rotor disk of order $\Omega t=0(\tau^{1/3})$, with t measured about $t=0$ (which corresponds to $\psi=90°$ in the usual rotor notation). For a blade with thickness ratio $\tau=0.06$ and μ between 0.2 and 0.4, the transonic sector has a total extent of about 45°, or 22.5° either side of $\psi=90°$ and $t=0$.

Equations (21) and (22) are not convenient for numerical calculations. A more convenient set of equations results by simply replacing S and T by y and t according to the definitions Eqs. (19) and (20). The result is

$$2M^2\frac{\epsilon}{\tau^{2/3}}(y+\mu\cos t)\phi_{xt}$$

$$=\left[\frac{1-M^2(y+\mu\cos t)^2}{\tau^{2/3}}-(\gamma+1)M^2\right.$$

$$\left.\times(y+\mu\cos t)\phi_x\right]\phi_{xx}+\frac{2M^2\epsilon}{\tau^{2/3}}\mu\sin t$$

$$\times(y+\mu\cos t)\phi_{xy}+\frac{\epsilon^2}{\tau^{2/3}}\phi_{yy}+\phi_{zz} \tag{23}$$

and

$$\phi_z=(y+\mu\cos t)f_x\ \text{for}\ Z=0 \tag{24}$$

These two equations describe transonic flow in the tip region and remain valid inboard through the subsonic strip theory region.

Although Eqs. (23) and (24) provide a properly scaled description of both the transonic and subsonic regions of flow, numerical experiments with unsteady two-dimensional flows show that rate of convergence of solutions is substantially increased by including additional time derivatives in Eq. (23), while the solution is unchanged. This advantage appears to carry over to three-dimensional unsteady calculations. Thus, the differential equation actually used in computations is

$$\frac{M^2\epsilon^2}{\tau^{2/3}}\phi_{tt}+2M^2\frac{\epsilon}{\tau^{1/3}}(y+\mu\cos t)\phi_{xt}$$
$$=\left[\frac{1-M^2(y+\mu\cos t)^2}{\tau^{2/3}}-(\gamma-1)M^2\epsilon\phi_t\right.$$
$$\left.-(\gamma+1)M^2(y+\mu\cos t)\phi_x\right]\phi_{xx}$$
$$+\frac{2M^2\epsilon}{\tau^{1/3}}\mu\sin t(y+\mu\cos t)\phi_{xy}$$
$$+\frac{\epsilon^2}{\tau^{2/3}}\phi_{yy}+\phi_{zz} \qquad (25)$$

The inclusion of the first term on the left-hand side of Eq. (25) and the ϕ_t term in the coefficient of ϕ_{xx} is not justified on order-of-magnitude grounds; but, as noted previously, their inclusion has a curious and beneficial effect on convergence rate.

Numerical Solution

Equation (25) was solved by extending the Murman method of Ref. 5 to the present case. The computational molecule is shown in Fig. 2. Stability requires ϕ_{xx} to be central-differenced in the subsonic region,

$$\phi_{xx}^{\text{central}}=\frac{1}{Dx^2}\left\{\phi^n_{i+1,j,k}-2\phi^n_{i,j,k}+\phi^n_{i-1,j,k}\right\}$$

whereas backward differences are required in the supersonic region:

$$\phi_{xx}^{\text{backward}}=\frac{1}{Dx^2}\left\{\phi^n_{i,j,k}-2\phi^n_{i-1,j,k}+\phi^n_{i-2,j,k}\right\}$$

where i,j,k refer to the x,y,z directions, respectively, and n refers to a time step t. At a shock point, the sum of the previous expressions is used to insure a conservative system in steady flow. This scheme has not been modified for the unsteady case studied here. The solution is stable whether central or mixed differencing is used for the terms involving streamwise derivatives, ϕ_{xt} and ϕ_{xy}. In our case, central differencing was used throughout for the ϕ_{xy} term:

$$\phi_{xy}=\frac{1}{(Dx)\ (Dy)}\left\{\phi^n_{i+1,j+1,k}+\phi^n_{i-1,j-1,k}\right.$$
$$\left.-\phi^n_{i+1,j-1,k}-\phi^n_{i-1,j+1,k}\right\}$$

This differencing results in a somewhat faster convergence rate than for mixed differences. Mixed differences were used for the ϕ_{xt} term:

$$\phi_{xt}=\frac{\phi^{n+1}_{i+1,j,k}+\phi^{n-1}_{i-1,j,k}-\phi^{n-1}_{i+1,j,k}-\phi^{n+1}_{i-1,j,k}}{(Dx)\ (Dt)} \qquad \text{for } M_\ell>1$$

$$\phi_{xt}=\frac{\phi^{n+1}_{i,j,k}+\phi^{n-1}_{i-1,j,k}-\phi^{n-1}_{i,j,k}-\phi^{n+1}_{i-1,j,k}}{(Dx)\ (Dt)} \qquad \text{for } M_\ell<1$$

where M_ℓ is the local Mach number.

Although central differencing in x is more convergent, it results in slightly irregular solutions just ahead of advancing shocks. This seems to be a consequence of trying to difference across a moving discontinuity—a situation that is eliminated by the switch to backward differencing. It is interesting to note that this problem never occurs when the shock moves rearward (in the accelerating flow region) since this is always a much slower process than is the reverse motion. (It should be noted that this switching can destroy flux conservation and cause errors in the computed shock speeds.) Backward differences are used for all time derivatives,

$$\phi_{tt}=\frac{1}{(Dt)^2}\left\{\phi^n_{i,j,k}-2\phi^{n-1}_{i,j,k}+\phi^{n-2}_{i,j,k}\right\}$$

Central differences were used in the spanwise and normal directions.

The system of nonlinear algebraic equations derived from the preceding differences was solved by use of successive over-relaxation (SOR). In order to start the solution, the first two time planes are computed, using the quasisteady equations at points in which the flow is well subcritical. When this is done, the solution is quite independent of where it is started. In the course of solution, an initial guess for the solution at each time step is made by a combined linear and quadratic extrapolation from the previous three time steps. In the course of solution, the relaxation factors used are a function of time. In the cases to be shown, the supersonic relaxation factor was always about 0.6. The subsonic relaxation factors varied from 1.85 initially to 1.3 at the maximum tip Mach number. These numbers are lower than is customarily the case because of the time derivatives. When the time step is decreased, the relaxation factors (and the convergence rate) drop markedly. However, the initial guess is so improved that the total computation time is almost independent of the time-step size used. The size of the x,y,z,t mesh array is usually about $60\times30\times30\times80$. On the CDC 7600, a typical computation time is presently about 45 min. It should be noted that no attempt was made to take advantage of the pipeline capability of this machine. Furthermore, SOR is by no means the fastest iterative method; it is, however, the simplest. The number of iterations per time step typically is about 20. This is very small compared to steady calculations.

As with steady calculations, the inboard boundary (at which two-dimensional flow is assumed) is about four chords from the tip, the outboard boundary is three chords removed, and the boundary perpendicular to the z-axis is about five chords removed. The downstream boundary is about two

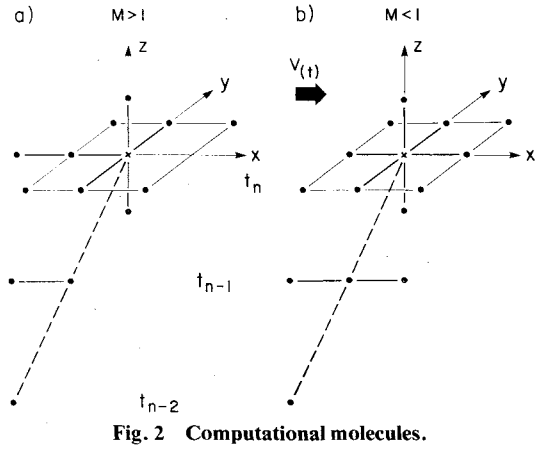

Fig. 2 Computational molecules.

chords removed from the trailing edge. However, the upstream boundary is exceptional, and is located no less than ten chords from the leading edge. This is because two-dimensional calculations show the emission of an upstream moving wave when the flow progresses from supercritical back down to subcritical. In order to resolve this wave adequately, a large number of mesh points were placed ahead of the profile (about 22). The resulting scarcity of points on the profile [Eq. (26)] is the main reason for restricting ourselves to the circular arc profile. As usual, for nonlifting solutions, the potential at the outer boundary is set equal to zero.

Results

Figure 3 shows a typical two-dimensional calculation. It depicts the decelerating portion of the flow ($\psi = 90°$) on a rotor, assuming strip theory to be valid. The three features that strike one are the suddenness with which the flow decelerates from supercritical to subcritical flow, the unusually (for a circular arc profile) far forward location of the maximum expansion in the course of this deceleration, and, finally, the upstream wave, which makes its appearance just as the collapse of the supersonic flow occurs. Figure 4 shows the full three-dimensional result for this same rotor. Although the flow is (as expected) far less expanded ($C_{p_{min}}$ at each time is less and the shock does not reach the trailing edge), the deceleration to subcritical flow looks much like the two-dimensional result. However, it occurs sooner in three-dimensions and, when it does, there is no upstream wave seen. This wave has, in fact, been seen in higher Mach number three-dimensional calculations; but its amplitude was about two orders of magnitude less than that seen in Fig. 1.

In order to distill results such as the preceding, it is convenient to plot the maximum Mach number (M_{max}) and the center of pressure ($X_{c.p.}$) of the flow. The reader should keep in mind that we are referring to the center of pressure of an absolute pressure distributions, rather than of the differential pressure across a lifting airfoil. Figure 5 shows the variation of these quantities (for unsteady and quasisteady calculations) as a function of azimuth angle for a three-dimensional calculation.. When supercritical flow just begins, it is seen that the only difference between the quasisteady and unsteady flows is a slight rearward shift of the latter pressure distribution. The maximum shock strength for the unsteady flows is a slight rearward shift of the latter pressure distribution. The maximum shock strength for the unsteady flows do not appear greatly different. However, the latter pressure distribution is shifted rearward, as seen in the center of pressure plot (Fig. 5). In fact, for this airfoil, the center of pressure seems to be a very good indicator of unsteadiness. This is seen in the subsequent point noted in this figure. At $\psi = 132°$, the center of pressure has moved to its most forward location indicative of a maintenance forward shift of the

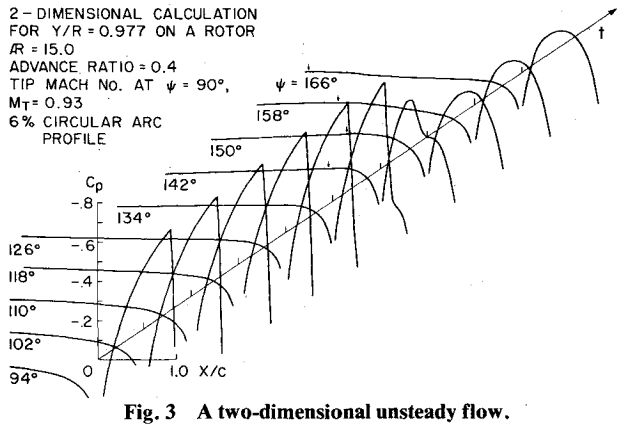

Fig. 3 A two-dimensional unsteady flow.

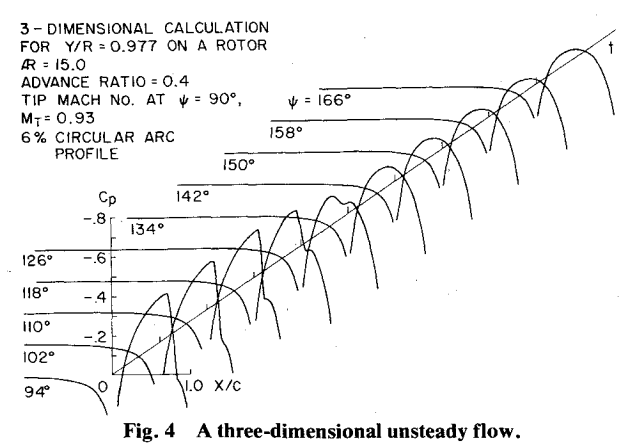

Fig. 4 A three-dimensional unsteady flow.

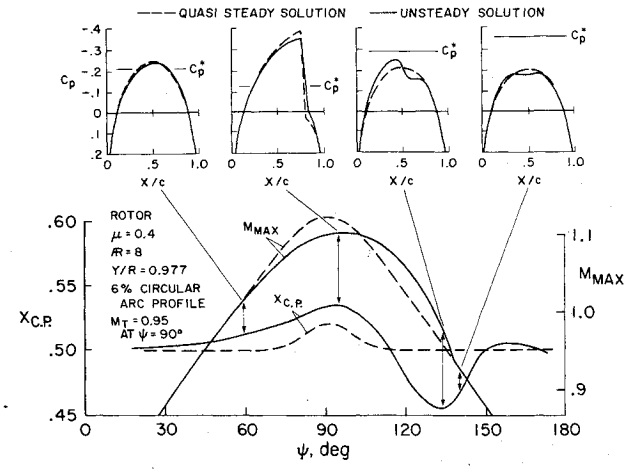

Fig. 5 A typical correlation of flow details with M_{max} and X_{cp} history.

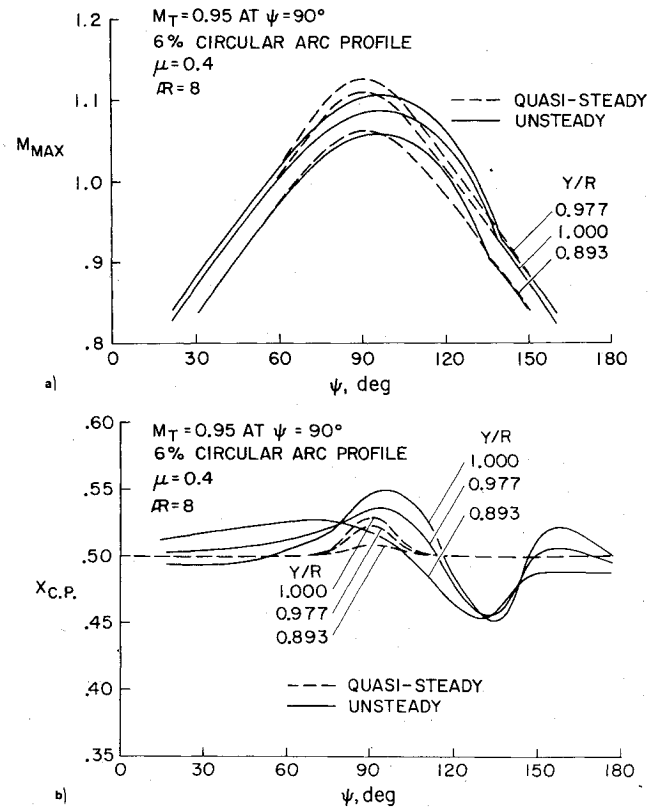

Fig. 6 a) Unsteady and quasisteady three-dimensional calculations. b) Concluded.

supersonic region and shock. According the the value of C_p^* at this point, the flow actually would appear to have become subcritical. This, however, ignores the fact that the pressure distribution is unsteady and an upstream moving shock could in fact have a subcritical flow—relative to the blade on both sides of the shock. This forward shift of the blade loading on deceleration is the most prominent consequence of unsteadiness to be seen in these calculations. Qualitatively similar results have been obtained by Beam and Ballhaus for the case of a lifting two-dimensional profile.[6] Finally, at the next point noted, this vestige of the forward loading has almost dissipated. There is a second minimum in the pressure distribution which again is getting close in appearance to the quasisteady distribution. The appearance of this second minimum is the reason for the kink that occurs on the decelerating side of the maximum Mach-number curve. This same association of pressure distribution with $X_{c.p.}$ and M_{max} time histories could have been made for any of the computed cases to be shown.

Figures 6a and 6b show the M_{max} and $X_{c.p.}$ plots for several span stations on a rotor. All stations show the same sort of retardation in M_{max} between the quasisteady and unsteady results, the most inboard returning to the quasisteady value somewhat sooner than the others. Also the trend for M_{max} as a function of span shows that expected tip relief. It is interesting that the rearward shift of the pressure distribution increases steadily out to the tip. The forward shift, which occurs on flow deceleration, does not vary greatly, but is seen to attain its maximum forward location at a greater aximuth angle as the tip is approached.

The effect of varying advance ratio is shown in Fig. 7. There are two competing effects at work here. On the one hand, increasing advance ratio causes greater unsteadiness in the flow and a reduction in peak expansion from what would be attained in quasisteady flow. On the other hand, increasing the advance ratio also increases the spanwise extent of the transonic flowfield on the blade, and therefore tends to increase the peak expansion. Figure 7 shows that the latter effect is the more important in that increasing the advance ratio increases the peak expansion. The higher advance ratio case also displays a greater forward shift in the center of pressure. However, the effect of changing advance ratio over a range that is greater than what is usually encountered in practice is seen not to be very great.

Figure 8 shows the effect of varying the maximum tip Mach number. The effect is clearly great. The maximum shock strength increases markedly for the higher Mach number. Also, the flow is obviously much more unsteady, since not only are the $X_{c.p.}$ excursions much greater, but the point of minimum $X_{c.p.}$ is markedly delayed for the higher Mach number cases. It is for this latter case that the upstream wave was noticed.

The effect of aspect ratio for a given thickness ratio (and hence of ϵ/π) is seen in Fig. 9. Concerning the reduction in the amount of flow expansion, the effect of reducing aspect ratio is seen to be considerable. However, the reduction in unsteadiness, as indicated by the forward $X_{c.p.}$ shift, appears to be small. Of course the lower aspect ratio flow really is the better one at this point, since it has the low M_{max}, and hence lower adverse pressure gradient. The effect of aspect ratio having this sort of mixed behavior is anticipated by the complicated role it plays in the governing equation. However, the point made in Ref. 1 concerning the desirability of low aspect ratio for transonic rotor flows appears to remain valid.

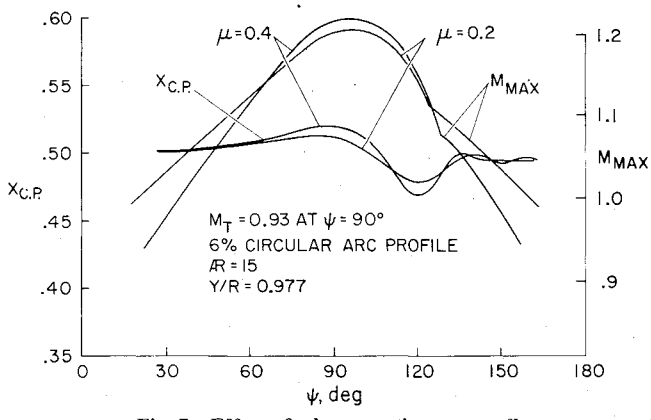

Fig. 7 Effect of advance ratio on rotor flow.

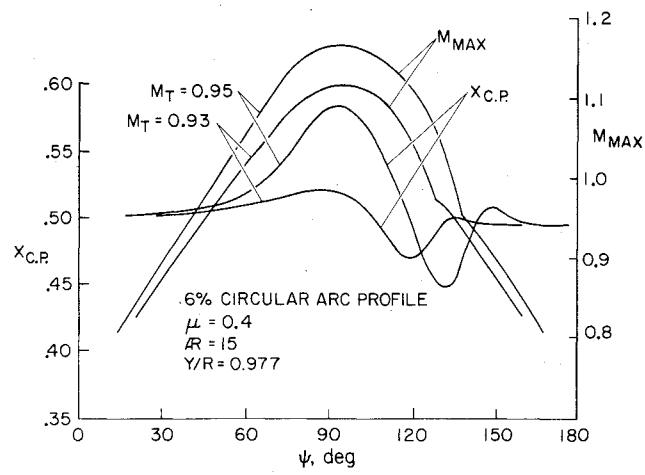

Fig. 8 Effect of Mach number on rotor flow.

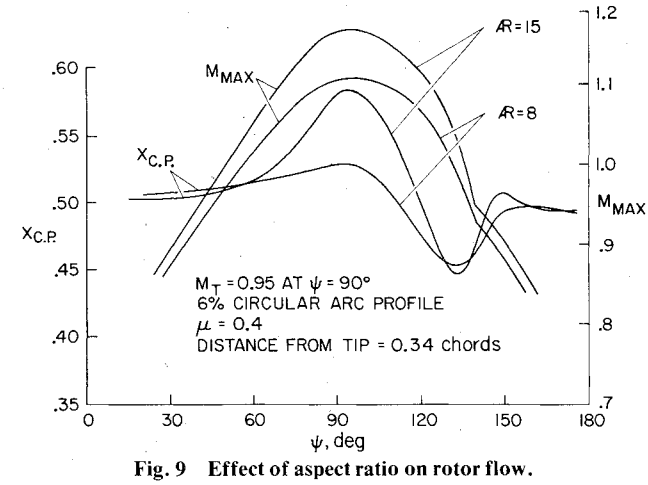

Fig. 9 Effect of aspect ratio on rotor flow.

Conclusions

The unsteady flow calculations seem to indicate the following results: 1) Supercritical flow on the advancing blade is likely to be accompanied by nonnegligible unsteadiness for very ordinary values of advance ratio. 2) The greatest difference between the unsteady and quasisteady flow occurs on the decelerating portion of flow (in the second quadrant), where a noticeable expansion and compression moves far forward on the chord. 3) Reduction of aspect ratio alleviates shock loss and unsteadiness. 4) Those parameters that are conducive to increasing the peak quasisteady supercritical expansion (advance ratio and especially Mach number and aspect ratio) also increase the unsteadiness.

Although it cannot now be stated absolutely, it is reasonable to assume that variations in rotor planform will have a similar effect. These conclusions suggest that quasisteady theory is probably the tool to use for blade design. It will not, however, give us all the important flow details and prediction of blade loads will require the unsteady theory.

Having neglected lift, much remains to be done in this investigation. However, many of the results presented here for the transonic nonlifting problem appear to be unusual and suggestive, and a fresh experimental investigation of the problem is warranted.

References

[1]Caradonna, F. X. and Isom, M. P., "Subsonic and Transonic Potential Flow over Helicopter Rotor Blades," *AIAA Journal*, Vol. 10, Dec. 1972, pp. 1606-1612.

[2]Krupp, J. A. and Murman, E. M., "Computation of Transonic Flows Past Lifting Airfoils and Slender Bodies," *AIAA Journal*, Vol. 10, July 1972, pp. 880-886.

[3]Ballhaus, W. F. and Caradonna, F. X., "The Effect of Planform Shape on the Transonic Flow Past Rotor Tips," *Aerodynamics of Rotary Wings, AGARD Conference Proceedings No. 111*, Feb. 1973.

[4]Isom, M. P., "Unsteady Subsonic and Transonic Potential Flows Over Helicopter Rotor Blades," NASA CR-2463, Oct. 1974.

[5]Murman, E. M., "Analysis of Embedded Shock Waves Calculated by Relaxation Methods," *Proceedings of AIAA Computational Fluid Dynamic Conference*, Palm Springs, Calif., July 19-20, 1973.

[6]Beam, R. and Ballhaus, W., "Numerical Integration of the Small-Disturbance Potential and Euler Equations for Unsteady Transonic Flow," NASA SP No. 347, March 1975.